Gray-box modeling of 300 mm diameter Czochralski single-crystal Si production process*

Shota Kato[a], Sanghong Kim[b,*], Manabu Kano[a], Toshiyuki Fujiwara[c], Masahiko Mizuta[c]

[a] *Department of Systems Science, Kyoto University, Yoshida-Honmachi, Sakyo-ku, Kyoto 606-8501, Japan*
[b] *Department of Chemical Engineering, Kyoto University, Nishikyo-ku, Kyoto 615-8510, Japan*
[c] *SUMCO Corporation, 1-52, Yamashiro-cho Kubara, Imari-shi, Saga 849-4256, Japan*

Abstract

More than 95% of 300 mm diameter single-crystal silicon ingots, the raw material for semiconductors, are produced by the Czochralski process. The demand for improving yield, throughput, and control performance has been increasing. The present study developed a gray-box model that can predict controlled variables from manipulated variables with higher accuracy than the conventional first-principle model (Zheng *et al.*, 2018), aiming at realizing model predictive control of the Czochralski process. The proposed gray-box model used a statistical model to predict the temperature gradient of the crystal at the solid-liquid interface G_{cry}, which was constant in the first-principle model. The crystal length and the melt temperature are used as the input variables to predict G_{cry}. The prediction accuracy of the proposed gray-box model was compared with that of the first-principle model using real process data obtained during the production of four silicon ingots. The results demonstrated that the proposed model reduced the root mean square errors of the crystal radius, the crystal growth rate, and the heater temperature by 94.1%, 62.7%, and 70.6% on average, respectively.

*This research did not receive any specific grant from funding agencies in the public, commercial, or not-for-profit sectors.

*Corresponding author
Email address: kim@cheme.kyoto-u.ac.jp (Sanghong Kim)

Keywords: A1. Gray-box model, A1. Growth models, A2. Czochralski method, A2. Single crystal growth, A2. Industrial crystallization, B2. Semiconducting Silicon

1. Introduction

Today, the use of electronic devices has increased with the spread of the Internet of Things, artificial intelligence, big data analysis, and cloud computing; consequently, the need for semiconductors has increased. According to the SEMI Silicon Manufacturers' Group (SMG), the shipments of silicon materials for semiconductor applications continued to increase from 2012 to 2018 [1]. As of 2009, more than 95% of single crystal silicon ingots with a diameter of 300 mm were manufactured by the Czochralski (CZ) process [2]. Demand for semiconductors and silicon ingots is expected to increase in the future; thus, improving the yield and throughput of the CZ process is crucial. Besides, higher quality silicon wafers are required as semiconductor devices become sophisticated.

A schematic diagram of the CZ process is shown in Fig. 1. In the CZ process, polycrystalline silicon is first filled into a crucible and melted by a heater. Then, a seed of the crystal is attached to the surface of the melt. By rotating and raising the crucible and the crystal, the crystal grows at the solid-liquid interface, and a single-crystal silicon ingot is obtained. The present study

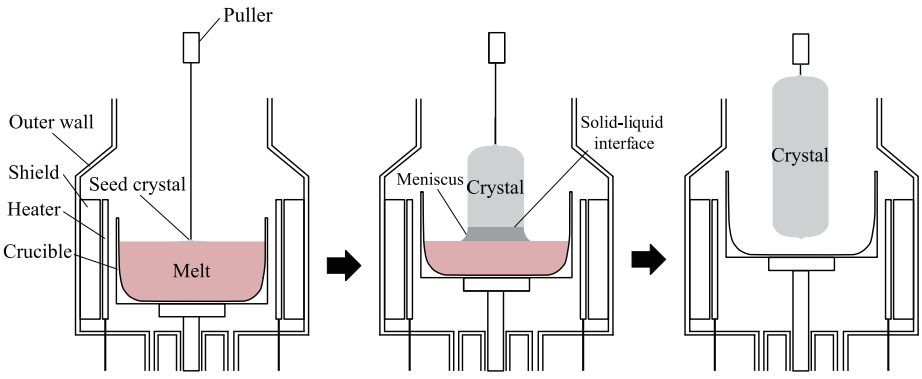

Fig. 1: Schematic diagram of the CZ process.

focuses on the duration of producing the ingot body. It is essential to control the crystal radius and the crystal growth rate to be constant to produce high-quality products. It is also necessary to control the position of the melt surface and the heater temperature so that the thermal environment around the solid-liquid interface does not change rapidly. Therefore, the controlled and manipulated variables shown in Table 1 are used in the industrial CZ process.

The CZ process is characterized by a long time constant between the heater input power and the controlled variables. Also, the input-output relationship changes over time due to the decrease in melt volume with crystal growth, and the relationship is nonlinear because the radiative heat transfer is dominant in the furnace. In the industrial CZ process, cascade control using PID controllers has been employed. Model predictive control (MPC) is expected to achieve higher control performance than the conventional PID control because MPC can cope with the nonlinear and time-varying relationship.

Table 2 summarizes the models of CZ processes for the control system design in previous studies. Gevelber and Stephanopoulos [3] developed a physical model representing the relationship between P, v_{p}, and r_{cry}. Winkler *et al.* [4, 5] and Neubert *et al.* [6] derived a physical model representing the relationship between v_{p}, v_{c}, and r_{cry}, by taking into account the mass balance and geometric relationship. Satunkin [7] developed a model based on the mass conservation

Table 1: Controlled variables and manipulated variables of the industrial CZ process.

Controlled variables	Crystal radius	r_{cry}
	Crystal growth rate	v_{g}
	Heater temperature	T_{h}
	Melt surface position	p_{mel}
Manipulated variables	Crystal pulling rate	v_{p}
	Crucible rise rate	v_{c}
	Heater input power	P

law, the heat balance, and the thermodynamic equilibrium condition at the three-phase line, with v_{p} and melt temperature T_{mel} as inputs and r_{cry} and meniscus height h_{men} as outputs. Abdollahi *et al.* [8, 9] constructed a physical model to represent the relationship between P, v_{p}, r_{cry}, and T_{mel}, considering the radiative heat transfer from the heater and the conductive heat transfer in the crystal. Rahmanpour *et al.* [10] developed a simple model with fewer states and parameters than the above models, with P and v_{p} as inputs and r_{cry} and T_{mel} as outputs. All of the above models were built for ingot production processes with a diameter of less than 200 mm. Since 300 mm diameter single-crystal silicon ingots are currently mass-produced, a model that can represent the dynamic characteristics of the industrial-scale CZ process is required [11]. Lee *et al.* [12] and Zhang *et al.* [13] constructed models whose input and output are T_{h} and v_{p}. Zheng *et al.* [14] developed a first-principle model to compute r_{cry} and v_{g} from P, v_{p}, and v_{c} for a process to produce 300 mm diameter single-crystal silicon ingots, and showed that the model simulated r_{cry} and v_{g} with high accuracy using real process data.

None of the previous models can accurately predict four controlled variables: r_{cry}, v_{g}, T_{h}, and p_{mel}. For the Czochralski silicon crystal process, the position of the melt surface is fixed during the crucible rise and the crystal growth. We can predict p_{mel} with high accuracy if v_{g} and r_{cry} are predicted with high accuracy because p_{mel} can be calculated from the mass balance of silicon. Thus, the objective of the present study is to develop a model to accurately estimate the three controlled variables (r_{cry}, v_{g}, and T_{h}) from the three manipulated variables of the CZ process. As pointed out by Zheng *et al.* [14], the prediction performance of the conventional lumped-parameter models is limited when applied to 300mm ingots. To realize the high prediction accuracy of r_{cry} and v_{g}, they proposed to divide the heater, the crucible, and the shield into three parts. We developed a gray-box model based on their first-principle model, and therefore, it can describe the phenomena of the 300 mm process better than the conventional models even though it is a lumped-parameter model. We further improved the first-principle model in the following points:

Table 2: Input and output variables and the target crystal diameter of the models built for the control system design of the CZ process in previous studies. The model type is either physical (P), statistical (S), or gray-box (G).

Reference	Model type	Input variable	Output variable	Crystal diameter [mm]
[3]	P	P, v_{p}	r_{cry}	40
[4, 5, 6]	P	v_{p}, v_{c}	r_{cry}	55
[7]	P	v_{p}, T_{mel}	r_{cry}, h_{men}	80
[8, 9]	P	P, v_{p}	r_{cry}, T_{mel}	100
[10]	P	P, v_{p}	r_{cry}, T_{mel}	160
[12]	S	T_{h}	v_{p}	200, 300
[13]	S	T_{h}	v_{p}	300
[14]	P	P, v_{p}, v_{c}	r_{cry}, v_{g}	300
Present study	G	P, v_{p}, v_{c}	r_{cry}, v_{g}, T_{h}	300

1. A systematic method for determining the initial conditions is developed.
2. The proposed model can predict T_{h} as well as r_{cry} and v_{g} with high accuracy by predicting the temperature gradient in the crystal at the solid-liquid interface.

Throughout this paper, we call the first-principle model consisting of an energy transfer model and a hydrodynamic and geometrical model, as the EHG model, and call the proposed model as the gray-box EHG (gray-EHG) model.

2. EHG model of CZ process

Figure 2 shows the structure of the EHG model. In the energy transfer model, the crystal growth rate v_{g} is calculated from the heater input power P, the crystal pulling rate v_{p}, and the crucible rise rate v_{c}. In the hydrodynamic and geometrical model, the crystal radius r_{cry} at the solid-liquid interface is calculated from v_{p}, v_{c}, and v_{g}. Details of each model are given in the following sections.

2.1. Energy transfer model

As shown in Fig. 3, the CZ process is assumed to consist of eight components: a crucible, a heater, a shield, a furnace bottom, melt, a meniscus section, a crystal, and an environment. To build a simple model that predicts the controlled variables with required prediction accuracy, we made some assumptions in modeling; for example, the heights of the shield and the heater are the same. The shield, the heater, and the crucible are divided into upper, middle, and lower parts. The height of each part is determined by the melt surface position and the crucible bottom position. The upper part, the middle part, and the lower part are represented by 1, 2, and 3, respectively. The energy balance of the crucible, the heater, the shield, the furnace bottom, the melt, and the meniscus section is calculated from the radiative heat transfer, conductive heat transfer, and heater input power. $Q_{i,j}$ is the radiative heat transfer from component i to component j, denoted by the solid arrow. $Q^*_{i,j}$ is the conductive heat transfer from component i to component j, indicated by the dotted arrow. Each heat transfer is calculated using the temperature of the components i and j. Subscripts "c," "h," "s," "b," "mel," "men," "cry," and "e" mean the crucible, the heater, the shield, the furnace bottom, the melt, the meniscus section, the crystal, and the environment, respectively. In the energy transfer model, the temperatures at the middle part and the lower part of the heater, $T_{\mathrm{h}(2)}$ and $T_{\mathrm{h}(3)}$, are assumed to be the same to build a simple model that satisfies the required prediction accuracy. The variables representing the radius r and the height h of each cylindrical component of the CZ process are shown in Fig. 4,

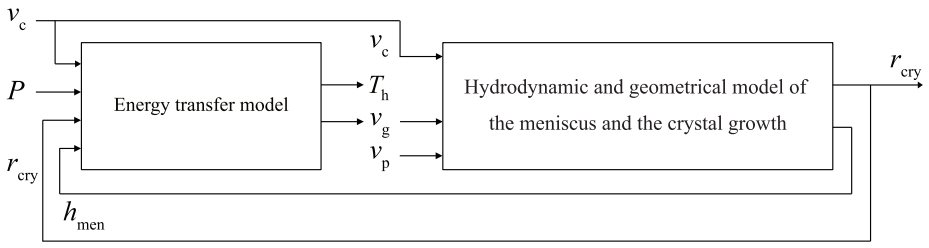

Fig. 2: Structure of the EHG model.

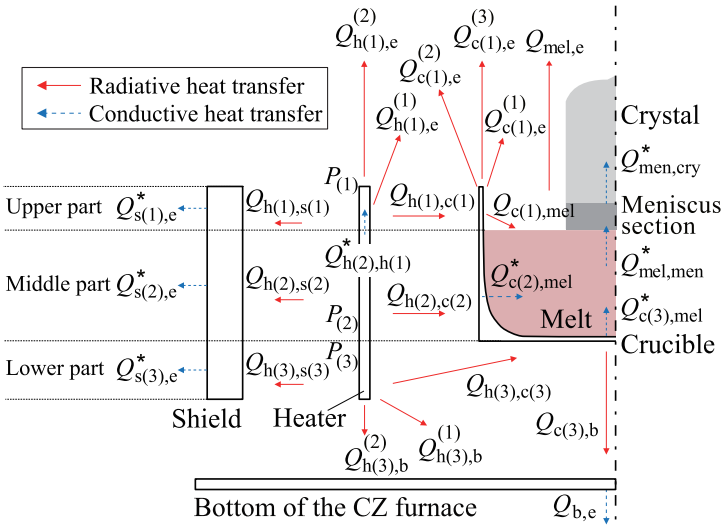

Fig. 3: Heat transfer calculated in the energy transfer model.

in which "in" and "out" represent the inside and outside parts. The amount of melt decreases with crystal growth, and the crucible rises to maintain a fixed position of the melt surface. Therefore, the upper, middle, and lower heights and the radius of the melt surface vary with the change of the melt surface position and the crucible position.

A quasi-steady state is assumed for the temperature of the shield, the crucible, and the furnace bottom to reduce the complexity and computational cost. Based on the assumption, the energy balance at the shield, the crucible, and the furnace bottom are expressed by

$$Q_{\mathrm{h}(k),\mathrm{s}(k)} - Q^{*}_{\mathrm{s}(k),\mathrm{e}} = 0 \qquad (k = 1, 2, 3), \tag{1}$$

$$Q_{\mathrm{h}(1),\mathrm{c}(1)} - Q_{\mathrm{c}(1),\mathrm{mel}} - Q_{\mathrm{c}(1),\mathrm{e}} = 0, \tag{2}$$

$$Q_{\mathrm{h}(2),\mathrm{c}(2)} - Q^{*}_{\mathrm{c}(2),\mathrm{mel}} = 0, \tag{3}$$

$$Q_{\mathrm{h}(3),\mathrm{c}(3)} - Q^{*}_{\mathrm{c}(3),\mathrm{mel}} - Q_{\mathrm{c}(3),\mathrm{b}} = 0, \tag{4}$$

$$Q_{\mathrm{h}(3),\mathrm{b}} + Q_{\mathrm{c}(3),\mathrm{b}} - Q^{*}_{\mathrm{b},\mathrm{e}} = 0. \tag{5}$$

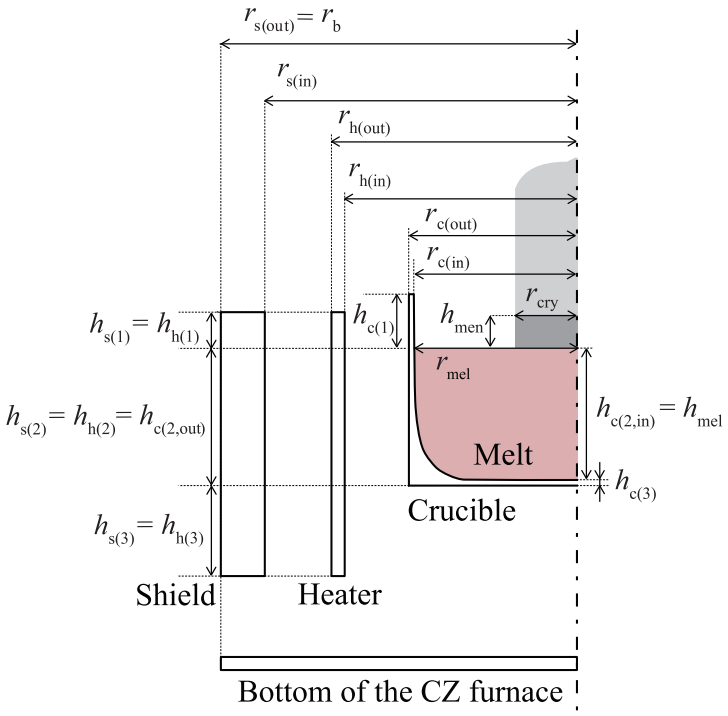

Fig. 4: Definition of the radius and the height of each component of the Czochralski process.

The energy balance of the heater is given by

$$\begin{aligned} C_{\mathrm{h}} \frac{\mathrm{d}h_{\mathrm{h}(1)} T_{\mathrm{h}(1)}}{\mathrm{d}t} &= P_{(1)} - Q_{\mathrm{h}(1),\mathrm{s}(1)} - Q_{\mathrm{h}(1),\mathrm{e}} + Q^*_{\mathrm{h}(2),\mathrm{h}(1)} \\ &\quad + C_{\mathrm{h}} \left((1-\delta_{\mathrm{h}}) T_{\mathrm{h}(1)} \frac{\mathrm{d}h_{\mathrm{h}(1)}}{\mathrm{d}t} + \delta_{\mathrm{h}} T_{\mathrm{h}(2)} \frac{\mathrm{d}h_{\mathrm{h}(1)}}{\mathrm{d}t} \right), \end{aligned} \tag{6}$$

$$\begin{aligned} C_{\mathrm{h}} \frac{\mathrm{d}\left(h_{\mathrm{h}(2)} + h_{\mathrm{h}(3)}\right) T_{\mathrm{h}(2)}}{\mathrm{d}t} &= \sum_{k=2}^{3} \left(P_{(k)} - Q_{\mathrm{h}(k),\mathrm{s}(k)} - Q_{\mathrm{h}(k),\mathrm{c}(k)} \right) \\ &\quad - Q^*_{\mathrm{h}(2),\mathrm{h}(1)} - Q_{\mathrm{h}(3),\mathrm{b}} \\ &\quad - C_{\mathrm{h}} \left((1-\delta_{\mathrm{h}}) T_{\mathrm{h}(1)} \frac{\mathrm{d}h_{\mathrm{h}(1)}}{\mathrm{d}t} + \delta_{\mathrm{h}} T_{\mathrm{h}(2)} \frac{\mathrm{d}h_{\mathrm{h}(1)}}{\mathrm{d}t} \right), \end{aligned} \tag{7}$$

$$C_{\mathrm{h}} = c_{\mathrm{h}} \rho_{\mathrm{h}} \pi \left(r^2_{\mathrm{h(out)}} - r^2_{\mathrm{h(in)}} \right), \tag{8}$$

$$P_{(k)} = \frac{h_{\mathrm{h}(k)}}{h_{\mathrm{h}}} P = \frac{h_{\mathrm{h}(k)}}{h_{\mathrm{h}(1)} + h_{\mathrm{h}(2)} + h_{\mathrm{h}(3)}} P \quad (k = 1, 2, 3), \tag{9}$$

$$\delta_{\mathrm{h}} = \begin{cases} 1 & \left(\frac{\mathrm{d}h_{\mathrm{h}(1)}}{\mathrm{d}t} \geq 0\right) \\ 0 & \left(\frac{\mathrm{d}h_{\mathrm{h}(1)}}{\mathrm{d}t} < 0\right) \end{cases}, \tag{10}$$

where $T_{i(k)}$ is the temperature of the part i of the component k. c_{h} and ρ_{h} are the specific heat and the density of the heater.

The energy balance of the melt can be described as follows:

$$c_{\mathrm{mel}} m_{\mathrm{mel}} \frac{\mathrm{d}T_{\mathrm{mel}}}{\mathrm{d}t} = Q_{\mathrm{c}(1),\mathrm{mel}} + Q^*_{\mathrm{c}(2),\mathrm{mel}} + Q^*_{\mathrm{c}(3),\mathrm{mel}} - Q_{\mathrm{mel,e}} - Q^*_{\mathrm{mel,men}}, \tag{11}$$

where c_{mel}, m_{mel}, and T_{mel} are the specific capacity, the mass, and the temperature of the melt.

In the energy transfer model, the axial thermal gradient in the meniscus section is assumed to be constant. Also assumed is that the radial thermal gradients in the crystal and the meniscus section are zero. Under the above assumptions, the crystal growth rate can be expressed as follows from the energy balance at the solid-liquid interface between the meniscus section and the crystal:

$$v_{\mathrm{g}} = \frac{k_{\mathrm{men}} G_{\mathrm{men}} - k_{\mathrm{cry}} G_{\mathrm{cry}}}{\rho_{\mathrm{cry}} \Delta H_{\mathrm{f}}}, \tag{12}$$

$$G_{\mathrm{men}} = -\frac{T_{\mathrm{mel}} - T^*}{h_{\mathrm{men}}}, \tag{13}$$

where k_{men} and k_{cry} are the heat conductivity of the meniscus section and the crystal. G_{men} and G_{cry} are the axial thermal gradients of the meniscus section and the crystal at the solid-liquid interface, ρ_{cry} is the density of the crystal, and ΔH_{f} is the specific latent heat of fusion for silicon. T^* is the crystallization point of silicon equal to the temperature at the solid-liquid interface. In the energy transfer model, k_{men}, k_{cry}, ρ_{cry}, ΔH_{f}, T^*, and G_{cry} are constant. The meniscus height h_{men} is calculated with the hydrodynamic and geometrical model explained in Section 2.2. The details of the energy transfer model are described by Zheng *et al.* [14].

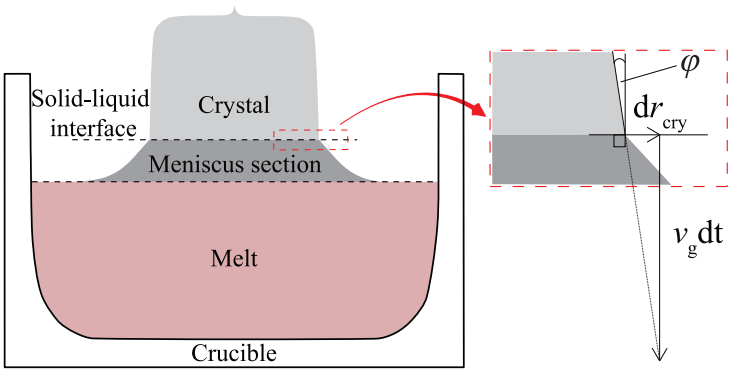

Fig. 5: Geometrical relationship around the solid-liquid interface.

2.2. Hydrodynamic and geometrical model

As shown in Fig. 5, r_{cry} is expressed by the following equation using v_{g} and the crystal slope angle φ [3]:

$$\frac{\mathrm{d}r_{\mathrm{cry}}}{\mathrm{d}t} = v_{\mathrm{g}} \tan(\varphi). \tag{14}$$

Equation (14) denotes that φ determines the direction of change in r_{cry}, since normally $v_{\mathrm{g}} > 0$. The crystal slope angle φ is expressed by the mass balance at the meniscus as follows:

$$\frac{\mathrm{d}\varphi}{\mathrm{d}t} = \frac{v_{\mathrm{p}} - v_{\mathrm{c}} - \psi_1(r_{\mathrm{cry}}, \varphi) v_{\mathrm{g}}}{\psi_2(r_{\mathrm{cry}}, \varphi)}, \tag{15}$$

where ψ_1 and ψ_2 are functions of r_{cry} and φ derived from the mass balance of silicon. Details of the derivation of ψ_1 and ψ_2 are described by Winkler *et al.* [4]. Ferguson proposed describing the meniscus height h_{men} with r_{cry} and φ [15]:

$$h_{\mathrm{men}} = a \sqrt{\frac{1 - \sin(\varphi_0 + \varphi)}{1 + \frac{1}{\sqrt{2} r_{\mathrm{cry}}}}}, \tag{16}$$

$$a = \sqrt{\frac{2\gamma}{\rho_{\mathrm{mel}} g}}, \tag{17}$$

where φ_0 is the wetting angle, γ is the surface tension of silicon, and g is the gravitational acceleration.

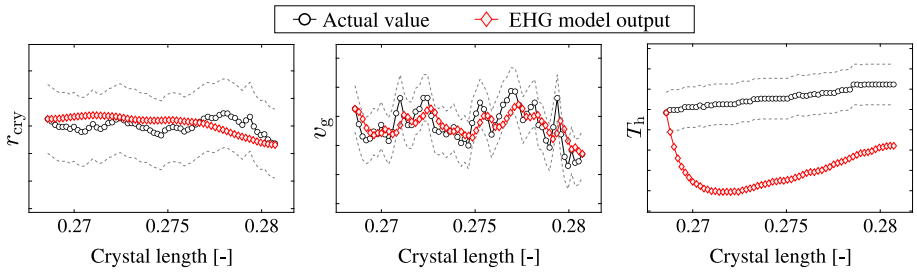

Fig. 6: Prediction result of the crystal radius r_{cry}, the crystal growth rate v_{g}, and the heater temperature T_{h} by the EHG model. The horizontal axis is the dimensionless crystal length. To protect confidentiality the scales of the vertical axis are shown in an arbitrary unit. The range between the dotted lines represents the tolerance of the prediction error.

2.3. Issue of EHG model

Figure 6 shows an example of the prediction results based on the EHG model. The heater temperature can be calculated as follows:

$$T_{\mathrm{h}} = \frac{h_{\mathrm{h}(1)} T_{\mathrm{h}(1)} + (h_{\mathrm{h}(2)} + h_{\mathrm{h}(3)}) T_{\mathrm{h}(2)}}{h_{(1)} + h_{(2)} + h_{(3)}}. \tag{18}$$

Figure 6 shows that r_{cry} and v_{g} can be predicted with high accuracy, while T_{h} cannot be accurately predicted. To improve the prediction accuracy of the three controlled variables, we focused on the temperature gradient at the solid-liquid interface G_{cry}, which is constant in the EHG model. Rahmanpour *et al.* [10] calculated the heat flux from the interface to the crystal ϕ_{s} using a computational fluid dynamics simulation software CGSim [16]. They showed that ϕ_{s} changed with the crystal length L. The result indicates that assuming G_{cry} as a function of L will improve the prediction accuracy of the controlled variables, because $k_{\mathrm{cry}} G_{\mathrm{cry}}$ corresponds to ϕ_{s} and k_{cry} is constant in this study.

3. Proposed gray-EHG model

As shown in Fig. 7, the proposed model consists of the EHG model and a statistical model. We construct the statistical model to predict the temperature gradient at the solid-liquid interface G_{cry} from the crystal length L and the melt temperature T_{mel} available in real-time.

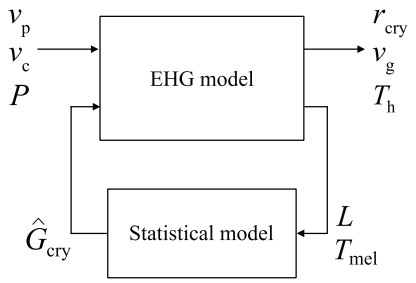

Fig. 7: Structure of the gray-EHG model.

3.1. Training data for statistical model

Before constructing the statistical model, we generated training data of G_{cry} because G_{cry} is unmeasurable. We calculated G_{cry} using the EHG model and real process data in the following methods. We adopted a quasi-steady-state assumption [17] that the crystal length changes much slower than the temperature of each process component and r_{cry}. This assumption leads to the following equations:

$$\frac{\mathrm{d}T_{\mathrm{h}(1)}}{\mathrm{d}t} = 0, \tag{19}$$

$$\frac{\mathrm{d}T_{\mathrm{h}(2)}}{\mathrm{d}t} = 0, \tag{20}$$

$$\frac{\mathrm{d}T_{\mathrm{mel}}}{\mathrm{d}t} = 0, \tag{21}$$

$$\frac{\mathrm{d}r_{\mathrm{cry}}}{\mathrm{d}t} = 0, \tag{22}$$

$$\frac{\mathrm{d}L}{\mathrm{d}t} = v_{\mathrm{g}}. \tag{23}$$

By replacing Eqs. (6), (7), and (11) in the energy transfer model with Eqs. (19)–(21), and using Eq. (22) and measurable process data (r_{cry}, v_{g}, h_{mel}, P, v_{p}, v_{c}, and crucible position p_{c}), we can calculate the temperature of each process component and φ. The following equation is obtained from Eqs. (12) and (13):

$$G_{\mathrm{cry}} = -\frac{1}{k_{\mathrm{cry}}}\left(\frac{k_{\mathrm{men}}(T_{\mathrm{mel}} - T^*)}{h_{\mathrm{men}}} + \rho_{\mathrm{cry}}\Delta H_{\mathrm{f}} v_{\mathrm{g}}\right). \tag{24}$$

G_{cry} is obtained by substituting the measured values of v_{g} and r_{cry}, and the calculated values of T_{mel} and φ into Eqs. (16) and (24).

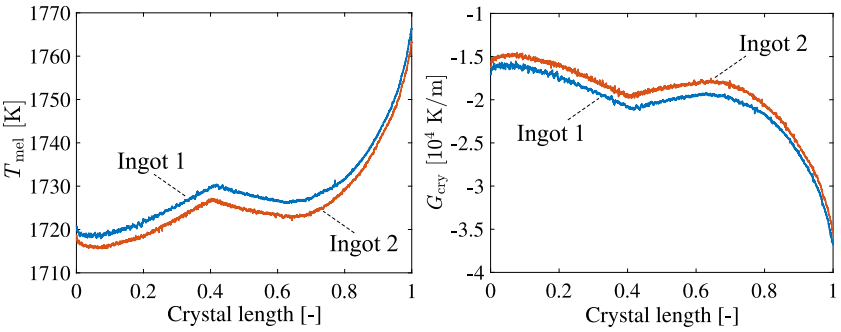

Fig. 8: Calculated melt temperature T_{mel} and temperature gradient in the crystal at the solid-liquid interface G_{cry} using the real process data of the ingots 1 and 2.

In the present study, we use real process data obtained during the production of six silicon ingots. The temperature of each process component and G_{cry} were calculated using the real process data of the ingots 1 and 2. We solved the algebraic equations by the trust-region method using MATLAB's function 'fsolve'. The calculated T_{mel} and G_{cry} are shown in Fig. 8. The range of $k_{\mathrm{cry}}G_{\mathrm{cry}}$ calculated using CGSim by Rahmanpour *et al.* [10] is -1.24×10^5 W/m^2 $\leq$ $k_{\mathrm{cry}}G_{\mathrm{cry}} \leq -1.04 \times 10^5$ W/m^2, and the range of $k_{\mathrm{cry}}G_{\mathrm{cry}}$ calculated from G_{cry} shown in Fig. 8 is -7.6×10^5 W/m^2 $\leq k_{\mathrm{cry}}G_{\mathrm{cry}} \leq -3.2 \times 10^5$ W/m^2. Although L and r_{cry} used by Rahmanpour *et al.* [10] are different from those used in the present study, $k_{\mathrm{cry}}G_{\mathrm{cry}}$ calculated from Fig. 8 are on the same order of that obtained by Rahmanpour *et al.* [10], and consequently, the derived values are considered to be reasonable.

3.2. Statistical model

When predicting the controlled variables, we need to calculate G_{cry} from variables that are known in real-time. We, therefore, construct a statistical model whose input variables are available in real-time, and the output variable is G_{cry}. Figure 8 shows that G_{cry} changes with the crystal length L, but it is not uniquely determined by L. In this study, we selected L and the melt temperature T_{mel} as the input variables $\boldsymbol{x}$ of the statistical model.

We employed Gaussian Process Regression (GPR) [18]

$$y = f_{\mathrm{GPR}}(\boldsymbol{x}) + \xi, \tag{25}$$

where y is an output variable, and ξ is a variable that follows a Gaussian distribution with zero mean and variance σ^2, and $f_{\mathrm{GPR}}(\boldsymbol{x})$ is a latent variable from a zero-mean Gaussian process with covariance function,

$$k(\boldsymbol{x}_n, \boldsymbol{x}_{n'} |\, \sigma_l, \sigma_f) = \sigma_f^2 \exp\left[-\frac{1}{2}\frac{(\boldsymbol{x}_n - \boldsymbol{x}_{n'})^{\mathsf{T}}(\boldsymbol{x}_n - \boldsymbol{x}_{n'})}{\sigma_l^2}\right], \tag{26}$$

where σ_l and σ_f are parameters, and $\boldsymbol{x}_n$ and $\boldsymbol{x}_{n'}$ are the nth and n'th samples of the input variables. In constructing the statistical model, the input and output variables were centered and scaled to have zero mean and unit variance. The parameters were determined by five-fold cross-validation.

3.3. Prediction accuracy of statistical model

We validated the statistical model constructed using the data of the ingot 1 by predicting G_{cry} of data of the ingot 2. The GPR model was derived by maximizing the likelihood with the subset of data points [18]. We used MATLAB's function 'fitrgp' to implement the algorithm. The prediction results in Fig. 9 show that the root-mean-square error (RMSE) was 2.5×10^2 K/m, and the determination coefficient R^2 was 1.0, confirming that the developed statistical model can estimate G_{cry} with high accuracy.

4. Results and Discussion

The prediction accuracy of the three controlled variables (the crystal radius r_{cry}, the crystal growth rate v_{g}, and the heater temperature T_{h}) by the EHG model and the proposed gray-EHG model was compared using real process data.

4.1. Simulation Conditions

To compare the prediction accuracy under different operating conditions, we applied the models to data of the ingots 3 to 6 that were obtained during

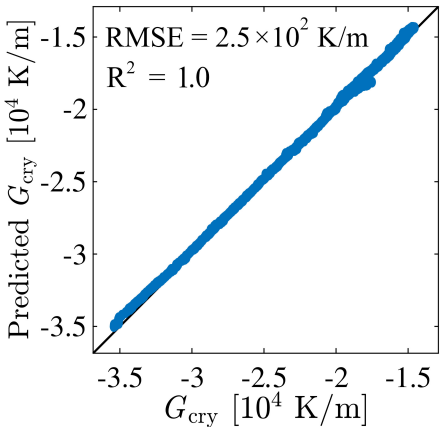

Fig. 9: Temperature gradient in the crystal at the solid-liquid interface G_{cry} predicted by the statistical model using the data of ingot 2.

the production of the ingot body. The data were divided without duplication into hourly subdata, and a total of 328 subdata (82 subdata per ingot) were used for validation. Figure 10 shows the input variables at three stages in the data of the ingot 3. Both models require the initial values of four variables: the crystal slope angle φ, the temperature at the upper part of the heater $T_{\mathrm{h}(1)}$, the temperature at the middle part of the heater $T_{\mathrm{h}(2)}$, and the melt temperature T_{mel}. In the previous study [14], the initial values were determined by trial and error to minimize the prediction error, because a systematic method for determining the initial values had not been developed. In this research, the initial values were calculated by the same method described in Section 3.1. In the EHG model, G_{cry} was calculated using Eq. (24) and process data (v_{g}, T_{mel}, and h_{men}) at the start of the prediction.

4.2. Prediction results

The statistical model in the proposed gray-EHG model was constructed using the training data generated from the data of the ingots 1 and 2. The parameters were determined by five-fold cross-validation; $\sigma = 0.01$, $\sigma_l = 5.43$, and $\sigma_f = 4.84$. We solved the algebraic differential equations using the bisection method and the Dormand-Prince method [19] to predict the controlled variables. The

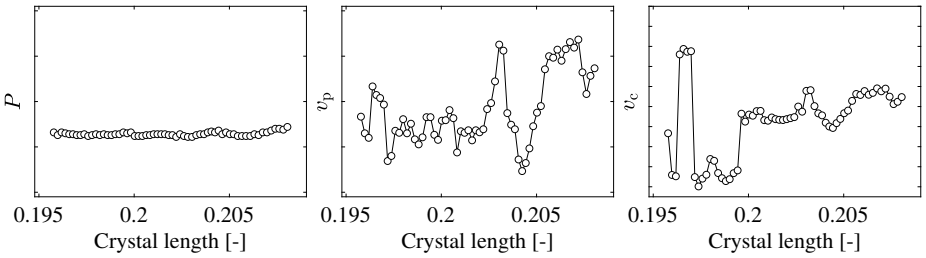

(a) Early stage.

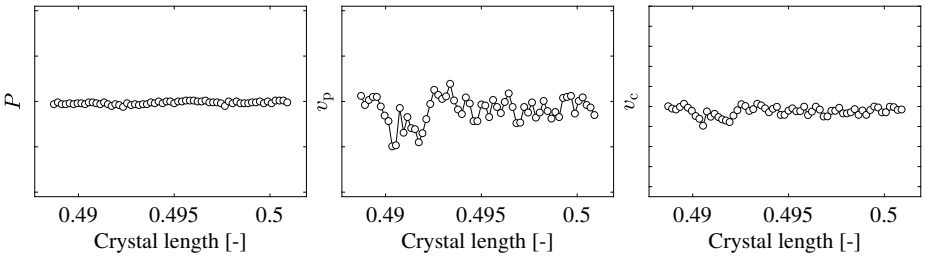

(b) Middle stage.

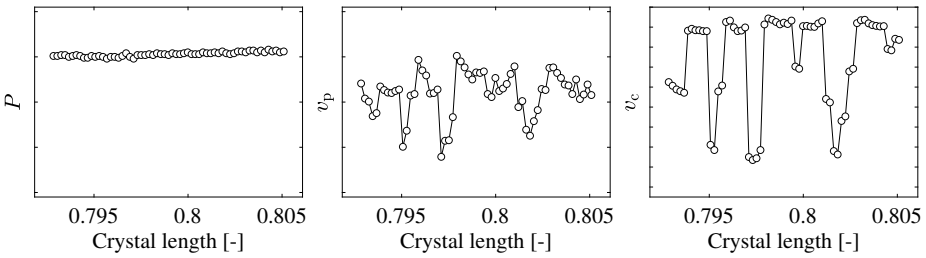

(c) Late stage.

Fig. 10: Input variables at three stages in data of the ingot 3. The values of the vertical axis are not shown to protect confidentiality.

algorithm was implemented using Simulink. The prediction accuracy of the controlled variables was evaluated based on the RMSE scaled by the acceptable error. Figure 11 shows the RMSE of each subdata against the crystal length at the start of the prediction. Figure 12 shows the prediction results of the controlled variables at three stages in the data of the ingot 3. In this research, v_g was defined as the moving average of the difference between v_p and the melt surface move rate. Table 3 shows that the mean value and standard deviation of the RMSEs of the gray-EHG model are smaller than those of the EHG model in

all cases. The proposed gray-EHG model reduced the mean of RMSEs of r_{cry}, v_{g}, and T_{h} by 93.7–94.4%, 56.2–69.2%, and 56.8–84.4%, respectively, compared to the EHG model.

Table 3: The mean and standard deviation of the RMSEs of three controlled variables: the crystal radius r_{cry}, the crystal growth rate v_{g}, and the heater temperature T_{h}.

Ingot	Model	RMSE of r_{cry}		RMSE of v_{g}		RMSE of T_{h}	
		mean	std	mean	std	mean	std
3	gray-EHG	0.38	0.21	0.64	0.25	0.83	0.53
	EHG	6.1	8.8	1.5	2.2	1.9	2.6
4	gray-EHG	0.37	0.25	0.61	0.27	0.86	0.54
	EHG	6.3	9.5	1.5	2.6	2.1	1.0×10^6
5	gray-EHG	0.37	0.21	0.55	0.27	0.69	0.51
	EHG	5.9	9.5	1.5	3.1	1.9	2.8
6	gray-EHG	0.36	0.18	0.51	0.26	0.78	0.50
	EHG	6.3	15	1.7	5.0	5.0	30

4.3. Discussion

The EHG model can accurately predict r_{cry} and v_{g} when the initial values of the four variables (φ, $T_{\mathrm{h}(1)}$, $T_{\mathrm{h}(2)}$, and T_{mel}) were determined by trial and error as shown in Fig. 6. The initial values were calculated by the method described in section 3.1; hence, the prediction accuracy of the EHG model was decreased for r_{cry} and v_{g}. On the other hand, the gray-EHG model can accurately predict the three controlled variables. Figure 13 shows that G_{cry} changes by about 1% in an hour in the gray-EHG model. These results show that predicting the change in G_{cry} based on the operating conditions is essential to achieve high prediction accuracy of the controlled variables. The prediction accuracy was significantly improved at the late stage, where the change of G_{cry} against the crystal length is larger than that at the other stages.

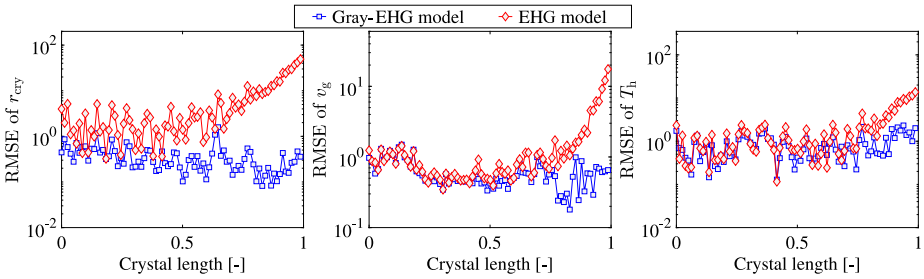

(a) Ingot 3.

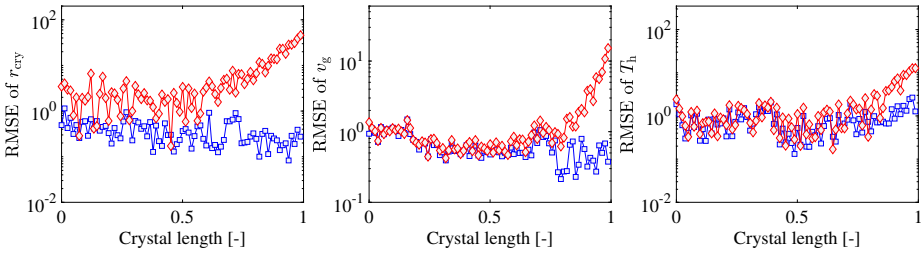

(b) Ingot 4.

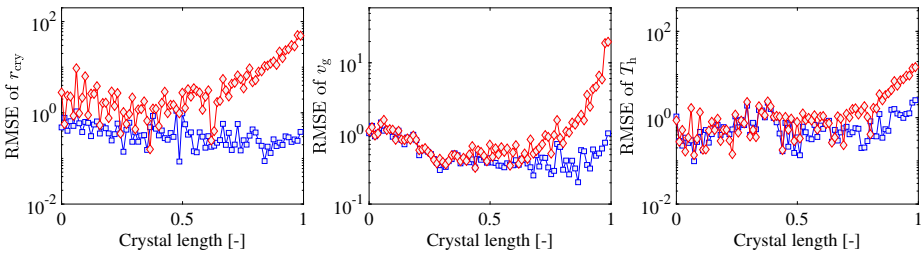

(c) Ingot 5.

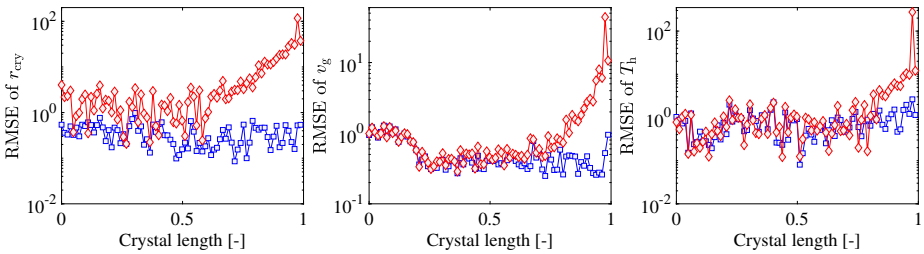

(d) Ingot 6.

Fig. 11: RMSEs of the crystal radius r_{cry}, the crystal growth rate v_{g}, and the heater temperature T_{h} against the data of the ingots 3 to 6. The horizontal axis is the dimensionless crystal length.

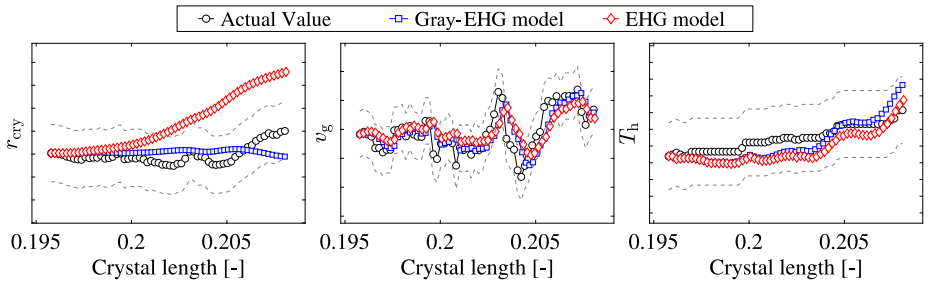

(a) Early stage.

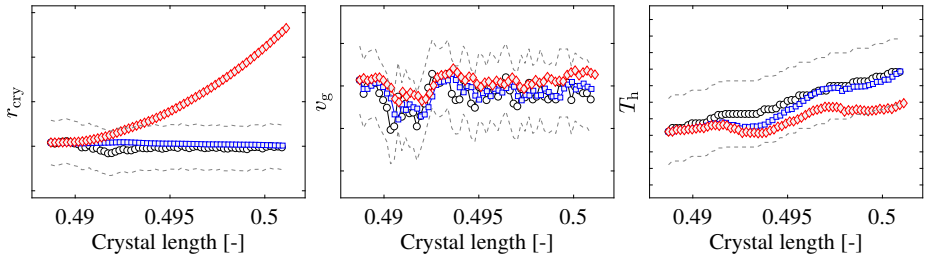

(b) Middle stage.

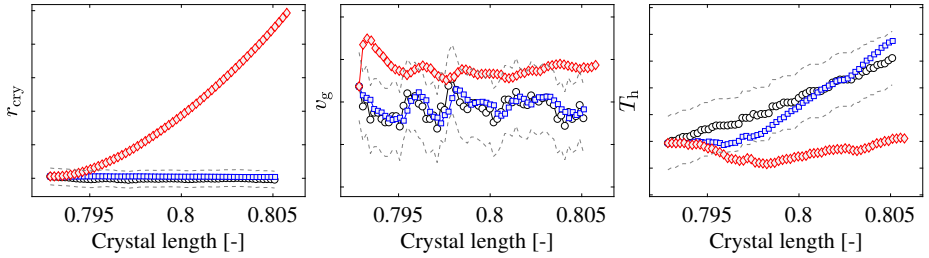

(c) Late stage.

Fig. 12: Prediction results of the crystal radius r_{cry}, the crystal growth rate v_{g}, and the heater temperature T_{h} at three stages in data of the ingot 3. To protect confidentiality the scales of the vertical axis are shown in an arbitrary unit. The range between the dotted lines shows an acceptable error.

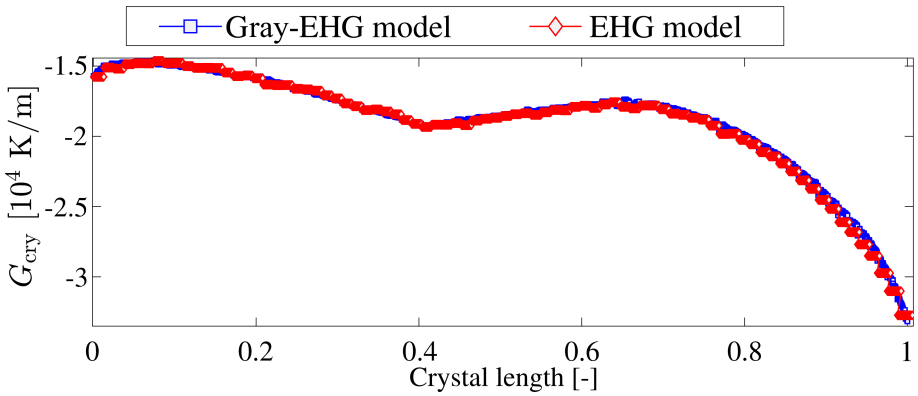

(a) All stages.

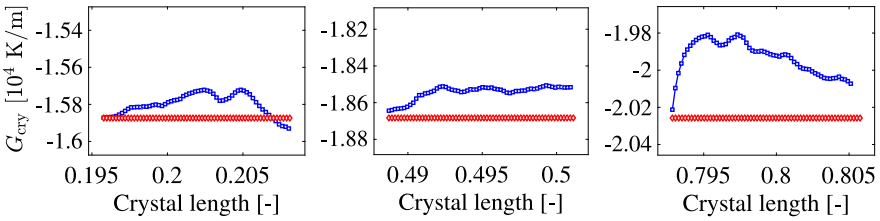

(b) Early stage. (c) Middle stage. (d) Late stage.

Fig. 13: Temperature gradient in the crystal at the solid-liquid interface G_{cry} used for prediction in the data of the ingot 3 by the EHG model and the gray-EHG model.

5. Conclusion

We developed a gray-box model that predicts the three controlled variables (r_{cry}, v_{g}, and T_{h}) with high accuracy, because the conventional first-principle model was not accurate enough to predict T_{h}. In the gray-box model, a statistical model is employed to predict the temperature gradient in the crystal at the solid-liquid interface G_{cry} from the crystal length and the melt temperature. The gray-box model and the first-principle model were validated using real process data. The gray-box model reduced the RMSEs of r_{cry}, v_{g}, and T_{h} by 94.1%, 62.7%, and 70.6%, compared to the first-principle model. A significant improvement in prediction accuracy was achieved, especially for the late phase of the batch, where G_{cry} changes faster than the other phases.

References

[1] Silicon shipment statistics — semi.org, http://www1.semi.org/en/MarketInfo/SiliconShipmentStatistics, accessed on 04/27/2020.

[2] L. Wu, Modeling and simulation of Czochralski bulk crystal growth process: investigation of transport effects in melt and gas phases, VDM Publishing, 2009.

[3] M. A. Gevelber, G. Stephanopoulos, Dynamics and control of the Czochralski process. I. Modelling and dynamic characterization, J. Cryst. Growth 84 (1987) 647–668. doi:10.1016/0022-0248(87)90056-X.

[4] J. Winkler, M. Neubert, J. Rudolph, Nonlinear model-based control of the Czochralski process I: Motivation, modeling and feedback controller design, J. Cryst. Growth 312 (2010) 1005–1018. doi:10.1016/j.jcrysgro.2009.12.074.

[5] J. Winkler, M. Neubert, J. Rudolph, Nonlinear model-based control of the Czochralski process II: Reconstruction of crystal radius and growth rate from the weighing signal, J. Cryst. Growth 312 (2010) 1019–1028. doi:10.1016/j.jcrysgro.2009.12.073.

[6] M. Neubert, J. Winkler, Nonlinear model-based control of the Czochralski process III: Proper choice of manipulated variables and controller parameter scheduling, J. Cryst. Growth 360 (2012) 3–11. doi:10.1016/j.jcrysgro.2012.03.018.

[7] G. Satunkin, Modelling the dynamics and control design for czochralski, liquid encapsulated czochralski and floating zone processes, Prog. Cryst. Growth Charact. Mater.56 (1-2) (2010) 1–121. doi:10.1016/j.pcrysgrow.2010.05.001.

[8] J. Abdollahi, S. Dubljevic, Crystal radius and temperature regulation in Czochralski crystallization process, in: Proceedings of the American Control Conference, 2013, pp. 1626–1632. doi:10.1109/ACC.2013.6580068.

[9] J. Abdollahi, M. Izadi, S. Dubljevic, Temperature Distribution Reconstruction in Czochralski Crystal Growth Process, AIChE Journal 60 (8) (2014) 2839–2852. doi:10.1002/aic.14486.

[10] P. Rahmanpour, S. Sælid, M. Hovd, O. Grønning, M. Jomaa, Nonlinear Model Predictive Control of the Czochralski Process, IFAC-PapersOnLine 49 (20) (2016) 120–125. doi:10.1016/j.ifacol.2016.10.107.

[11] M. Hourai, T. Nagashima, H. Nishikawa, W. Sugimura, T. Ono, S. Umeno, Review and comments for the development of point defect-controlled cz-si crystals and their application to future power devices, Phys. Status Solidi A 216 (10) (2019) 1970035. doi:10.1002/pssa.201800664.

[12] K. Lee, D. Lee, J. Park, M. Lee, MPC based feedforward trajectory for pulling speed tracking control in the commercial Czochralski crystallization process, Int. J. Control Autom. Syst. 3 (2) (2005) 252–257.

[13] J. Zhang, D. Liu, Y. Zhao, Gpc based adaptive crowning growth control in cz-si process, in: 2016 35th Chinese Control Conference (CCC), 2016, pp. 211–215. doi:10.1109/ChiCC.2016.7553085.

[14] Z. Zheng, T. Seto, S. Kim, M. Kano, T. Fujiwara, M. Mizuta, S. Hasebe, A first-principle model of 300 mm czochralski single-crystal si production process for prediction crystal radius and crystal growth rate, J. Cryst. Growth 492 (2018) 105–113. doi:10.1016/j.jcrysgro.2018.03.013.

[15] A. Ferguson, Lxxxix. on the shape of the capillary surface formed by the external contact of a liquid with a cylinder of large radius, Philos. Magaz. 24 (144) (1912) 837–844. doi:10.1080/14786441208634877.

[16] Cgsim package for modeling and optimization of crystal growth from the melt, `http://www.str-soft.com/products/CGSim/`, accessed on 04/27/2020.

[17] J. J. Derby, L. J. Atherton, P. D. Thomas, R. A. Brown, Finite-element methods for analysis of the dynamics and control of Czochralski crystal growth, J. Sci. Comput. 2 (4) (1987) 297–343. doi:10.1007/BF01061294.

[18] C. E. Rasmussen, C. K. Williams, Gaussian processes for machine learning, Vol. 2, The MIT Press, Cambridge, MA, 2006. doi:10.1007/978-3-540-28650-9_4.

[19] J. Dormand, P. Prince, A family of embedded runge-kutta formulae, J. Comput. Appl. Math. 6 (1) (1980) 19–26. doi:10.1016/0771-050X(80)90013-3.